Stacked Amorphous Silicon Color Sensors

Dietmar Knipp, Patrick G. Herzog, and Helmut Stiebig

***Abstract*—Color sensors based on vertically integrated thin-film structures of amorphous silicon (a-Si : H) and its alloys were realized to overcome color moiré or color aliasing effects. The complete color information of the color aliasing free sensors is detected at the same spatial position without the application of additional optical filters. The color separation is realized in the depth of the structure due to the strong wavelength dependent absorption of a-Si : H alloys in the visible range. The sensors consist of three stacked p-i-n diodes. The spectral sensitivity of the sensors can be controlled by the optical and electronic properties of the materials on one hand and the design of the devices on the other hand. In order to investigate the optical wave propagation within the device and to optimize the color separation we have developed an optical model, which takes the optical properties of the individual layers and the device design into account. The optical model has been combined with a colorimetric model, which facilitates the benchmarking of the color sensors and the reduction of the color error of the sensors. Finally, an improved device design will be presented.**

***Index Terms*—Amorphous materials, color, photo detectors, thin-film devices, thin films.**

I. Introduction

COLOR image processing is usually performed with the aid of color filter array (CFA)-coated charge-coupled device (CCD) or CMOS sensor arrays [1]. However, color detection with a CFA leads to the color moiré, or color aliasing effect, which is observed when structures with high spatial frequencies are captured. Additionally, traditional sensor systems exhibit low area fill factors, because one color pixel is split into several chromatic subpixels. In order to overcome the color moiré, effect, vertically integrated sensor structures have been proposed, which detect the color information in the depth of the sensor structure [2]–[9]. Furthermore, stacked sensor systems based on amorphous silicon (a-Si : H) can be integrated on top of amorphous, polycrystalline, or crystalline readout electronics [10]–[12], because a-Si : H can be prepared at low temperatures (200–300 °C).

The device design of the color sensors ranges from two-terminal thin-film devices [2]–[7], which change the spectral sensitivity as a function of the applied bias voltage, to multiterminal devices in thin-film or crystalline silicon technology [8], [9]. Two-terminal sensors can typically be described by an anti-serial connection of two diodes [5]–[7], a phototransistor configuration [2], or a diode with different absorption regions for the detection of red, green, and blue light [3], [4]. Since the spectral response can be shifted from blue to green and red by the variation of the applied voltage, the color channels must be separately selected and read out sequentially. The pixel pitch of amorphous two-terminal sensors integrated on top of a processing electronic is similar to CCD or CMOS sensors. A pixel pitch of $5 \times 5\ \mu\text{m}^2$ has been demonstrated for an a-Si : H black/white sensor on top of an application specific integrated circuit (ASIC) [12]. The area fill factor is close to 100%. Similar values can be expected for two-terminal color sensor arrays. Furthermore, it has be mentioned that two-terminal devices suffer from nonlinearities [3], because the spectral sensitivity depends on the intensity of the illumination. Additionally, real-time applications are limited by the transient response times, especially at low levels of illumination. This behavior originates from the trapping and recombination behavior of carriers in a-Si : H [3], [13].

To improve the linearity of the spectral response, we have realized thin-film devices based on three vertically integrated diodes of a-Si : H and its alloys. Since the diodes are driven at reverse bias, a good carrier extraction, a high linearity, and a fast response are achieved. Additionally, a stacked three-channel detector can be read out by one shot. Multiterminal devices are characterized by a more complex layer structure since four terminals have to be connected with the readout electronic of each pixel. This fact results in a lower area fill factor. Furthermore, the integration of three individual sensors facilitates a more flexible design of the absorption region to achieve an adjusted spectral sensitivity for red, green, and blue. Due to the device design, blue light is mainly absorbed in the top diode and green light in the second diode, whereas red light mainly determines the photocurrent of the bottom diode (see Fig. 1). In order to match the demands of different applications, the optical bandgap of the material can be controlled over a wide range by the deposition conditions. The color recognition of the sensors is in general limited by the mismatch between the spectral sensitivities of the sensor and the color matching curves representing human color vision [14]. Furthermore, a general limitation of a-Si : H-based color detectors is the broadened blue response, due to the high absorption of light for longer wavelength even for thin layers. This originates from the lack of absorption materials with a high optical bandgap ($>$2.3 eV) and good electrical properties. On the other hand, the thickness of the diodes can only be shortened to a certain extent, since decreasing the absorption layer thickness reduces the dynamic range. This is due to the decrease of the photocurrent and an increase of the dark current caused by microshunts. As a consequence, the spectral sensitivity of the top diode is widened and a decrease of the color error of the sensor is restricted.

Manuscript received May 29, 2001; revised September 25, 2001. The review of this paper was arranged by Editor K. Najafi.

D. Knipp was with the Research Center Jülich, Institute of Photovoltaics, 52425 Jülich, Germany. He is now with Xerox Corporation, Palo Alto Research Center, Palo Alto, CA 94304 USA.

P. G. Herzog is with Aachen University of Technology, Technical Electronics Institute, 52056 Aachen, Germany.

H. Stiebig is with the Research Center Jülich, Institute of Photovoltaics, 52425 Jülich, Germany.

Publisher Item Identifier S 0018-9383(02)00220-4.

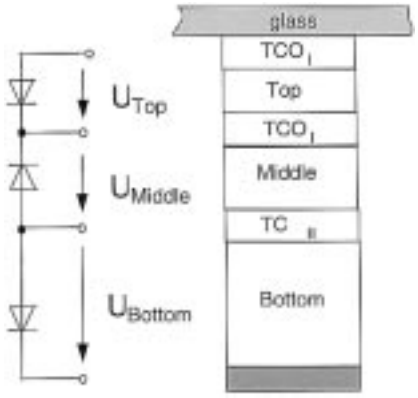

Fig. 1. Schematic configuration of a three-channel sensor based on three vertical integrated diodes.

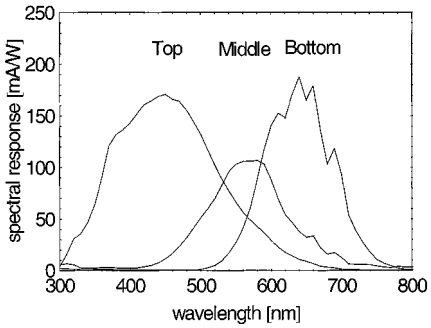

Fig. 2. Measured spectral response of a three-channel sensor based on three vertically integrated p-i-n diodes. The sensitivity is measured under short-circuit conditions.

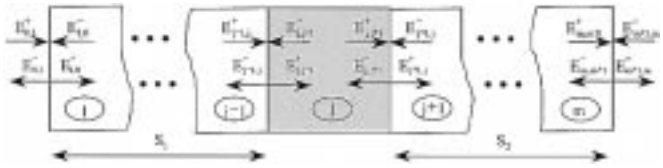

Fig. 3. Schematic sketch of a multilayer sequence based on the m-layer system.

In Section II, we describe the experimental realization of the vertically stacked color sensors. Experimental results will be presented in Section III. Based on the realized structure, in Section IV, we develop an optical model, which facilitates the calculation of the spectral sensitivity of each diode as a function of the design of the multilayer stack and the absorption materials in order to analyze the optical properties of the sensors. The optical simulations and the influence of the device design on the spectral sensitivity will be discussed in Section V. The colorimetric characterization of the sensor for different device designs will be discussed in Section VI and an improved and experimentally realized device structure will be discussed in Section VII. Finally, conclusions will be presented in Section VIII.

II. Experiment

The samples have been deposited in a multichamber plasma-enhanced chemical vapor deposition (PECVD) system at 210 °C on glass substrates coated with flat transparent conductive oxide (TCO). The TCO-layers have been realized by rf-magnetron sputtered zinc oxide [15]. Each of the three amorphous diodes consists of a p-i-n-layer structure. In order to vary the optical bandgap within the device, different layers were alloyed with carbon using a gas mixture of silane and methane. The optical bandgaps of the i-layers increase with enhanced carbon content. P- and n-type doped layers were realized by adding trimethylboron and phosphine, respectively. A detailed description of the deposition parameters can be found in [16]. The optical constants and the optical bandgap of the layers have been determined by a separated characterization of individual layers by transmission/reflection, constant photocurrent method (CPM), and ellipsometry measurements. After deposition of the complete layer stack (see Fig. 1) the samples were patterned using photolithography and reactive ion etching. In order to pattern the four-terminal devices, a simple three-mask process has been developed. We use thermally evaporated aluminum as a back contact. The area of the realized sensors varies between 3 and 10 mm^2 for all realized structures.

III. Experimental Results

In Fig. 2, the spectral response of a produced three-channel sensor is given. The three-channel sensor based on three vertically integrated diodes allows the simultaneous detection and readout of three sensor signals. The i-layer thickness of the top, middle, and bottom diode is approximately 85 nm, 200 nm, and 700 nm, respectively. The optical bandgap of the absorption layers in the top, middle, and bottom diode is 2.0 eV, 1.9 eV, and 1.75 eV, respectively, by alloying carbon to the deposition gas silane. The spectral response curves of the three-color detector (see Fig. 2), measured under short-circuit conditions, exhibit maximum at 450 nm, 560 nm, and 640 nm and full widths at half maximum (FWHM) of 185 nm, 125 nm, and 120 nm, respectively.

IV. Optical Model

To investigate different device designs, we have developed an optical model, which calculates the optical generation profile in a multilayer system as a function of the position and the wavelength. The optical wave propagation within a multilayer system can be calculated by different approaches [17]. One of the easiest ways to implement a mathematical method is the application of matrix formalism [18]. In the case of isotropic materials assuming smooth and parallel layers, a one-dimensional model can describe the wave propagation. This assumption leads to a drastically simplified mathematical formalism. In the applied matrix formalism the output of the system can be described by a linear function, which directly correlates the input and the output electric field vectors. A chain matrix S describes the transfer matrix of the multilayer system. The formalism is applied to the layer stack, shown in Fig. 3:

$$\begin{bmatrix} E^{+}_{0,1} \\ E^{-}_{0,1} \end{bmatrix} = \begin{bmatrix} s_{11} & s_{12} \\ s_{21} & s_{22} \end{bmatrix} \cdot \begin{bmatrix} E^{+}_{m+1,m} \\ E^{-}_{m+1,m} \end{bmatrix} = S \cdot \begin{bmatrix} E^{+}_{m+1,m} \\ E^{-}_{m+1,m} \end{bmatrix}. \quad (1)$$

The component $E^{+}_{0,1}$ describes the electric field toward the first interface in positive direction, whereas $E^{-}_{0,1}$ represents the electric field at the interface between layers 0 and 1 in negative di-

rection. The components $E_{m+1,m}$ indicate the electric output field at the interface between the $m-$ and $m+1$-layer. The layer $m+1$ is typically the back contact, so that $E^{-}_{m+1,m}$ becomes zero. The scattering matrix S describes the multilayer system

$$S = \begin{bmatrix} s_{11} & s_{12} \\ s_{21} & s_{22} \end{bmatrix} = \left(\prod_{\nu=1}^{m} I_{\nu-1,\nu} T_{\nu} \right) \cdot I_{m,m+1}. \quad (2)$$

The scattering matrix is set together by a step-by-step multiplication of interface (I) and transmission (T) matrix elements for each interface and each layer. Based on the scattering matrix the transmission and the reflection of the whole multilayer system can be determined. In order to simplify the description of the optical wave propagation, the layer stack can be divided into a three-layer system based on the j-layer and two subsystems S_1 and S_2. Hence, the description of the layer stack is simplified to a stack consisting of the subsystem S_1 (layer 1 to $j-1$), the layer j itself, and the subsystem S_2 (layer $j+1$ to m). Therefore, the transmissions and reflections of the subsystems can be defined.

Based on these expressions, the electric field in the j-layer can be calculated as a superposition of the electric field into positive and negative directions

$$\begin{aligned} E_j(x) &= E_j^{+}(x) + E_j^{-}(x) \\ &= \left(t_j^{+} \cdot e^{i\kappa_j x} + t_j^{-} \cdot e^{-i\kappa_j x} \right) \cdot E_{0,1}^{+} \end{aligned} \quad (3)$$

$t_{\delta}^{+/-}$ is the transmission through the j-layer in positive/negative directions. The intensity within the layer j can be calculated after a few transformations, as given in (4) and (5). I_0 is the incident light intensity and $T_j(\lambda) = \eta_j(\eta_0)^{-1}|t_j^{+}|^2$ corresponds to an internal transmission of the multilayer system. α_j is the absorption coefficient of the j-layer ($\alpha_j = 4\pi\kappa_j/\lambda$). ρ_2^{+} and ϕ_2^{+} denotes the absolute value and the phase of the reflection of the subsystem S_2, respectively

$$I_j(x,\lambda) = \tfrac{1}{2}\, c\varepsilon_0 \eta_j \left| E_j(x,\lambda) \right|^2 \quad (4)$$

$$\begin{aligned} I_j(x,\lambda) = I_0 T_j \Bigg(& e^{-\alpha_j x} + \left(\rho_2^{+}\right)^2 \cdot e^{-\alpha_j (2d_j - x)} + 2\rho_2^{+} \\ & \cdot e^{-\alpha_j d_j} \cdot \cos\left(\frac{4\pi\eta_j}{\lambda}(d_j - x) + \phi_2^{+} \right) \Bigg). \end{aligned} \quad (5)$$

The first term $e^{-\alpha_j x}$ of (5) originates from the electric field propagation into positive direction. The positive direction means the direction of the incident light. The second term $e^{-\alpha_j(2d_j - x)}$ describes the electric field propagation into negative direction. The third term is due to interference effects of the two waves. The interference component is especially important for very thin layer systems and/or systems with a distinct difference in the complex refractive indexes of the individual layers.

In the next section, we will show that the interference effects can be applied as a tool to improve the color separation, especially for the top diode of a vertically integrated three-color sensor. In order to determine the optical spectral sensitivity of the individual diodes, the optical energy dissipation has to be integrated over the active region (i-layer) of the diode. We assume that the collection efficiency of the carriers generated in the i-layer is 100%, because of the electric field in the thin active regions is high under short-circuit conditions and material with low defect density was incorporated.

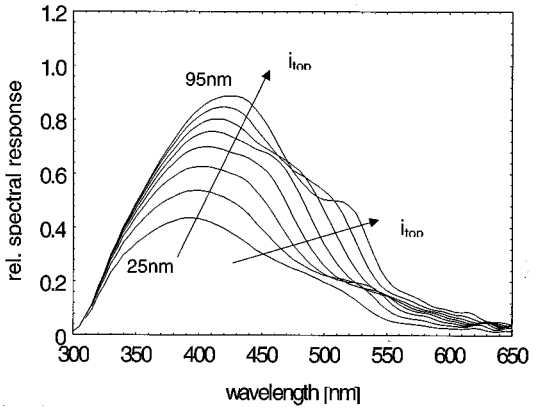

Fig. 4. Simulated and normalized spectral sensitivity of the top diode of a stacked three-color sensor. The applied optical bandgap of the absorption layer is 2.0 eV. The absorption layer thickness was varied from 25 nm to 95 nm.

V. Optical Simulations

A comparison of the realized sensor (see Fig. 1) with crystalline sensors covered with optical filters or with the color matching functions [14] indicates that the spectral response curves of the three channels (see Fig. 2) are widened. The difference in spectral sensitivity between the experimentally realized sensor and the standard observer [14] is caused by the lack of optoelectronic materials with a high optical bandgap and good optoelectronic properties. The available material limits especially the spectral sensitivity of the top diode. However, the shape of the spectral response in this range depends also on the device structure. Before the influence of the top diode layer thickness and the optical bandgap on the device performance was investigated, the reflection of the realized structure was calculated [19] to confirm the accuracy of the assumed device structure. The relative spectral response of the top diode as a function of the layer thickness is given in Fig. 4 for an optical bandgap of 2.0 eV.

The peak of the shown spectral sensitivities is normalized to the maximum value of the simulated spectral sensitivity of a structure with an i-layer thickness of 85 nm, which is correlated with the experimentally realized structure. In the simulation, the thickness was varied between 25 nm and 95 nm. This variation results in a shift of the maximum of the spectral response from 390 nm to 425 nm. However, the FWHM of the spectral response curves gives a comprehensive view of the simulation results (see Fig. 5).

The circles and squares in Fig. 5 indicate the FWHM of the top diode employing optical bandgaps of 2.0 eV and 2.2 eV, respectively. The reduction of the thickness of the absorption layer within the top diode from 85 nm (experimental) to 65 nm or 55 nm leads to a narrowing of the spectral response curve and a decrease of the FWHM by 15 nm down to 170 nm. For a thicker absorption layer ($d_i = 105$ nm), a reduction of the FWHM is

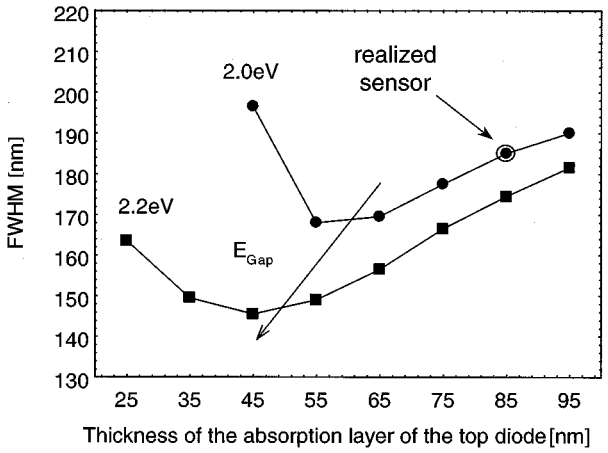

Fig. 5. FWHM of the simulated spectral response of the top diode of a vertical integrated three-channel sensor for different absorption layer thickness. The circles and squares correspond to optical bandgaps of 2.0 eV and 2.2 eV, respectively.

observed in the simulation. For an i-layer thickness thinner than 55 nm, an increase of the FWHM is also calculated. The variation of the FWHM is mainly determined by interference effects, which appear between 500 nm and 520 nm (see Fig. 4). As a consequence, the shape of the blue response for longer wavelength is changed. This can be explained by the third term in (5). The variation of the thickness from 55 nm or 65 nm to 95 nm leads to a change from destructive to constructive interference in the amorphous layers of the top diode for the wavelength of 500 nm, caused by a change of $\Delta d_j \eta_j = \lambda/4$. For calculations assuming an optical bandgap of 2.2 eV instead of 2.0 eV, a shift of the minimum of the FWHM down to 145 nm can be observed for an absorption layer with a thickness of 45 nm. Nevertheless, the shape of the blue response is similar. Based on the calculations in Fig. 5, the FWHM of the top diode can be reduced to a certain extent, but the influence of microshunts significantly enhances the dark $I-V$ current for very thin diodes.

VI. Colorimetric Characterization

Different models have been developed to transform the spectral sensitivity of stacked color sensors into standardized color formats (e.g., CIE) ranging from simple transformations of the spectral response curves [3], [4], [20] to colorimetric characterization models using sets of test colors [21]–[23]. Colorimetric characterizations of stacked color sensors have been performed using the spectral response data [21], [22] or experimental data determined by the characterization of color test charts [23].

In the following, a colorimetric characterization model based on the spectral response of the sensor will be applied to benchmark the performance of the produced and numerically calculated sensors. Based on the following equations, three color stimuli were calculated for the three sensor signals

$$V_d = k \cdot \int_{380\ \mathrm{nm}}^{780\ \mathrm{nm}} D(\lambda) \cdot r(\lambda) \cdot \omega_d(\lambda)\, d\lambda. \tag{6}$$

The suffix d denotes the three measured channels 1, 2, and 3 and the three color stimuli V_1, V_2, and V_3 are free of dimensions. $D(\lambda)$ is the spectral power distribution of the incident light, $r(\lambda)$ is the spectral reflection of the object, and ω is the spectral sensitivity of a channel of the sensor. k is a pre-factor to normalize the calculations to a white reference object. The integration was repeated for all three sensor channels. If $\omega_d(\lambda)$ in (6) is replaced by the color matching functions $\overline{x}(\lambda)$, $\overline{y}(\lambda)$, $\overline{z}(\lambda)$, the colorimetric tristimulus values X, Y, and Z are obtained. In order to obtain colorimetric values from the sensor outputs V_d, a transformation matrix A is set up, yielding

$$(X, Y, Z) = (V_1, V_2, V_3) \cdot A. \tag{7}$$

This procedure is repeated for all test colors. In the first step, a least square fit is used to determine the $3 \times 3 = 9$ parameters of the matrix A. A set of reference colors has been used for the fit. In the second step, the matrix A has been applied to calculate the estimated tristimuli for the sensor via (7). In this case, a set of test colors has been used. In the third step, the exact (standard observer) and the estimated values (sensor) are transformed into the CIELab color space, which is visually rather physically uniform. After the nonlinear transformation into the Lab color space, the color error for each individual test color can be determined by

$$\Delta E_{ab} = \sqrt{(L_S^* - L_D^*)^2 + (a_S^* - a_D^*)^2 + (b_S^* - b_D^*)^2}. \tag{8}$$

L_S and L_D represent the brightness of the CIE standard observer and the detector, respectively. The variables a_S, b_S, a_D, and b_D correspond to hue ($h = \arctan(b/a)$) and chroma ($c = (a+b)/2$) of the standard observer and the detector. In this case, ΔE_{ab} represents the color error in the CIELab color space. Based on the average color error and the root-mean-square of the evaluated test colors, different sensors can be compared regarding the color perception of the human eye. A more detailed description of the colorimetric characterization is given in [24].

The colorimetric characterization has been applied to the optically calculated spectral response curves of a vertically stacked three-color sensor. The color error for different thickness of the top diode is shown in Fig. 6, employing an absorption layer with an optical bandgap of 2.0 eV and 2.2 eV, respectively. A set of 1269 Munsell test colors has been used for the evaluation [20].

A good agreement between the color error for the simulated and realized structure is obtained. In contrast to the decreasing FWHM for the top diode, an increase of the color error is observed for the thinner i-layer. The reduction of the FWHM of the spectral response from 185 nm to 170 nm results in an increase of the average color error from $\Delta E_{ab} = 5.1$ to $\Delta E_{ab} = 5.4$. The lowest color error is calculated for top diodes with an optical bandgap of 2.2 eV in combination with an 80- or 90-nm thick absorption layer. However, the difference of the color error cannot only be explained by a change of the spectral sensitivity of the top diode. A modification of the design affects the transmission of light through the top diode as well. The spectral response of the middle diode is mostly affected by a change of the transmission through the top diode. The optical calculations of the spectral response point out that, only for very thin top diodes, a shift of the spectral response of the middle diode to shorter wavelengths is observed (see Fig. 7).

For a layer thickness in the top diode between 55 nm and 95 nm, the maximum of the spectral response curve of the middle

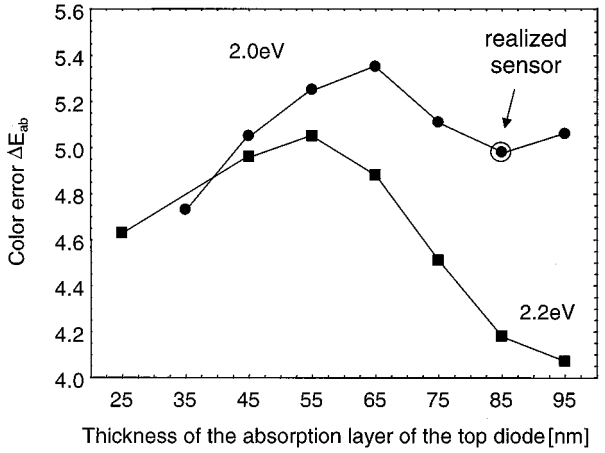

Fig. 6. Color error of three-channel sensor based on optical calculated spectral response curves as a function of the thickness of the absorption layer of the top diode. The circles and squares correspond to optical bandgaps of 2.0 eV and 2.2 eV, respectively.

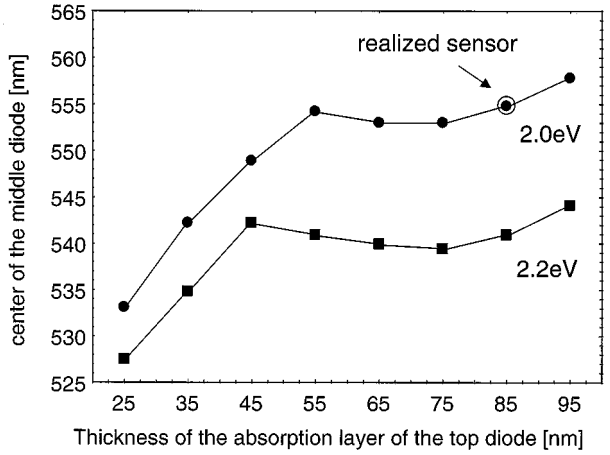

Fig. 7. Center of the middle diode of the three-color sensor based on optical calculated spectral response curves as a function of the thickness of the absorption layer of the top diode. The circles and squares correspond to optical bandgaps of 2.0 eV and 2.2 eV, respectively.

diode keeps constant at 555 nm and 540 nm, employing a material with bandgaps of 2.0 eV and 2.2 eV, respectively. This result confirms that interference effects mainly determine the change of the spectral sensitivity for the top diodes, whereas the direct absorption [terms 1 and 2 of (5)] is mainly unchanged. In order to understand the reduction of the color error for the top diode with an optical bandgap of 2.2 eV and a thickness of 85 nm or 95 nm, a second aspect has to be taken into account. The overlap of the spectral response curves is a further condition, which has an impact on the color error. A large or a very small overlap of the spectral response leads to an enhanced color error due to a mismatch of the spectral response curves and the color matching functions. The FWHM of the sensor in Fig. 2 is relatively large, especially for the top diode. Therefore, an enhancement of optical bandgaps from 2.0 eV to 2.2 V leads to a drastically decrease of the color error, whereas a further reduction of the thickness of the top diode leads to no further improvement ($d_i = 55$ nm/$E_g = 2.0$ eV, $d_i = 55$ nm/$E_g = 2.0$ eV). For thinner absorption layers in the top diode, a destructive interference at 500 nm takes place. As a consequence, the overlap of the spectral responses of the top

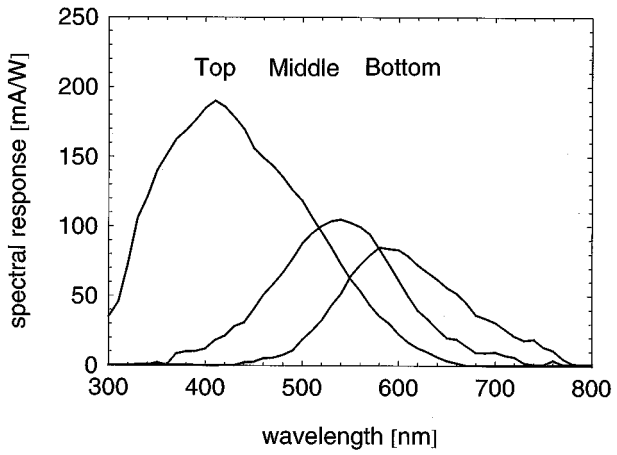

Fig. 8. Measured relative spectral response of a three-channel sensor based on three vertically integrated p-i-n diodes. The sensitivity is measured under short-circuit conditions.

TABLE I
THICKNESS AND OPTICAL BANDGAPS OF THE INCORPORATED AMORPHOUS SILICON ABSORPTION LAYERS WITHIN THE STACKED p-i-n DIODES AS WELL AS THE COLOR ERROR ΔE_{ab}, STANDARD DEVIATION σ, AND MAXIMUM COLOR ERROR $\Delta E_{\max}$ USING A SET OF 1269 TEST COLORS [20]

Sensor	Top Diode [d_i/E_g]	Middle Diode [d_i/E_g]	Bottom Diode [d_i/E_g]
Sensor A (experimental, Fig. 2)	85nm/2.0eV	205nm/1.9eV	700nm/1.75eV
Sensor B (simulated, Fig. 5, 6)	85nm/2.2eV	205nm/1.9eV	700nm/1.75eV
Sensor C (experimental, Fig. 8)	85nm/2.2eV	150nm/1.9eV	400nm/1.75eV
Sensor	**Color error [ΔE_{ab}]**	**Deviation [σ]**	**Max. error [ΔE_{max}]**
Sensor A (experimental, Fig. 2)	5.12	4.24	20.16
Sensor B (simulated, Fig. 5, 6)	4.18	2.98	16.35
Sensor C (experimental, Fig. 8)	3.6	3.06	33.92

diode and the middle diode is reduced. Based on the discussed optimization criteria, we have prepared a sensor structure with improved device design.

VII. IMPROVED DEVICE DESIGN

The properties of a stacked multichannel sensor with an optical bandgap of 2.2 eV in the top diode are depicted in Fig. 8. The maximum of the spectral sensitivity of the new top diode shifts from 450 nm to 410 nm due to the higher (2.2 eV) bandgap.

As a further comparison of Fig. 2 and Fig. 8 indicates, the optical bandgap of the top diode is not the only parameter, which has changed to optimize the sensor. A summary of the calculated color errors, standard deviations, and maximum errors of the different device structures is given in Table I. The thickness of the absorption layers of the middle and the bottom layer has also been reduced from 205 nm in the middle diode to 150 nm and from 700 nm to 400 nm in the bottom diode. Caused by the reduced thickness of the absorption layers, in particularly, the maximum of the red response shifts to shorter wavelengths and the absolute value of the spectral sensitivity is reduced. Hence, the red response of the sensor fits well with the standard observer for longer wavelength [15]. Consequently, the color error is lower than the calculated one in the previous section. Sensor A corresponds to the experimentally realized sensor in Fig. 2. The absorption layer of the top diode has a thickness of 85 nm and an optical bandgap of 2.0 eV. Sensor B is the optically simulated sensor using an absorption layer of 85 nm and a bandgap

of 2.2 eV in the top diode. The color error of Sensor C corresponds to the experimentally realized structure C. As mentioned above, the sensor consists of a top diode used for Sensor B ($d_i = 85$ nm/$E_g = 2.2$ eV) in combination with the modified absorption layer thickness of the middle and bottom diode. In addition to the modified design of the amorphous absorption layers, a surface treatment of the TCO-layer between the middle and the bottom diode was performed that drastically reduces the interference fringes of the third channel. A description of the texture process and the optical properties of the rough TCO-layer are given in [14]. The texture of the TCO-layer leads to a smoothing of the spectral response curve of the bottom diode and reduces the sensitivity to deviations of the thickness of the whole layer stack due to the fabrication process of the individual layers. However, experimental results and optical calculations reveal that the spectral sensitivity of the individual diodes is less sensitive to deviations of the absorption rather than changes in the thickness of the individual diodes due to fluctuations of the fabrication process. As mentioned, for the bottom diode of the stacked sensor, the sensitivity to interference effects can be reduced by the incorporation of a rough contact layer. Due to light scattering the contribution of coherent light propagation reduces. This approach can be also used for the middle diode, which leads to a slightly increase of the color error but improves the uniformity and the robustness of the fabrication process. However, the modification of the design of the middle and the bottom diode results in an additional reduction of the color error from $\Delta E_{ab} = 4.18$ to $\Delta E_{ab} = 3.6$. Furthermore, the standard deviation σ of the color error for the applied 1269 Munsell test colors has been distinctly reduced for Sensors B and C in comparison to Sensor A. Only the maximum color error of the novel device has been increased due to the shift of the maximum of the spectral response of the middle diode from 540 nm to 530 nm, and the shift of the maximum of the spectral response of the bottom diode from 640 nm to 590 nm. Nevertheless, the colorimetric calculations in Table I point out that the Sensor C in Fig. 8 is clearly superior to Sensor A in Fig. 2. To compare the realized sensor structures with other sensors, we have characterized several other digital cameras and scanners in respect to their color resolution. The color error of commercially available sensors is typically in the range of $\Delta E_{ab} = 3-4$. Therefore, the novel device structure demonstrates a color resolution, which is compatible and, in some cases, better than commercial sensors.

VIII. Conclusion

Novel color sensors based on stacked thin-film diodes have been developed. These thin-film structures enable color moiré, free color detection. Accordingly, the complete color information can be detected at the same position of a sensor array without the aid of optical filters. In order to match the demands of different applications, an optical model has been developed which describes the wave propagation within the multilayer stack. In combination with a colorimetric characterization model, a direct correlation between the optical design of the color sensor and the color error of the structure was established. Based on the optical and colorimetric calculations, a novel device design has been determined and a sensor has been experimentally realized. The ability to use interference effect engineering in the short wavelength range as a powerful tool to improve the performance of optical sensor has been described and demonstrated. The optimized sensor exhibits a color error comparable with commercial detectors using optical filters.

Acknowledgment

The authors would like to thank F. Finger, B. Rech, H. Siekmann, H. Wagner (Research Center, Jülich), J. Zimmer (Infineon, Muenich), F. Koenig (University of Technology, Aachen), H. J. Büchner (Technical University Ilmenau), and R.A. Street (Xerox PARC) for many helpful discussions and support.

References

[1] K. Engelhardt and P. Seitz, "Optimum color filters for CCD digital cameras," *Appl. Opt.*, vol. 32, no. 16, p. 3015, 1993.
[2] K. C. Chang, C.-Y. Chang, Y. K. Fang, and S. J. Jwo, "The amorphous Si/SiC heterojunction color-sensitive phototransistor," *IEEE Electron Device Lett.*, vol. EDL-8, pp. 64–66, Feb. 1987.
[3] J. Zimmer, D. Knipp, H. Stiebig, and H. Wagner, "Amorphous silicon-based unipolar detector for color recognition," *IEEE Trans. Electron Devices*, vol. 45, pp. 884–891, May 1999.
[4] D. Yang, K. S. Ambo, and J. W. Holm-Kennedy, "Four-color discriminating sensor using amorphous silicon drift-type photodiode," *Sens. Actuators*, no. 14, p. 69, 1988.
[5] H.-K. Tsai and S.-C. Lee, "Amorphous SiC/Si three-color detector," *Appl. Phys. Lett.*, vol. 52, no. 4, p. 275, 1988.
[6] G. de Cesare, F. Irrera, F. Lemmi, and F. Palma, "Tunable photodetectors on amorphous Si/SiC heterostructures," *IEEE Trans. Electron Devices*, vol. 42, pp. 835–843, May 1995.
[7] K. Eberhardt, T. Neidlinger, and M. B. Schubert, "Three-color sensor based on n-i-p-i-n-layer sequence," *IEEE Trans. Electron Devices*, vol. 42, pp. 1763–1772, Oct. 1995.
[8] D. P. Poenar and R. F. Wolffenbuttel, "Thin-film optical sensors with silicon compatible materials," *Appl. Opt.*, vol. 36, no. 21, p. 5109, 1997.
[9] P. Seitz, D. Leipold, J. Kramer, and J. M. Raynor, "Smart optical and image sensors fabricated with industrial CMOS/CCD semiconductor processes," *SPIE*, vol. 1900, p. 21, 1993.
[10] R. A. Street, "Large area image sensor arrays," in *Technology and Applications of Amorphous Silicon*. ser. Springer Series in Material Science, R. A. Street, Ed. Berlin, Germany: Springer-Verlag, 2000, vol. 37, pp. 147–217.
[11] J. Lu, K. van Schuylenbergh, R. T. Fulks, J. Ho, Y. Wang, R. Lau, P. Nylen, P. Mei, M. Mulato, J. B. Boyce, and R. A. Street, "Flat panel imagers based on excimer laser annealed poly-Si thin-film technology," in Proc. Material Research Society Symp., vol. 685, 2001, to be published.
[12] T. Lulé, S. Benthien, H. Keller, F. Mütze, P. Rieve, K. Seibel, M. Sommer, and M. Böhm, "Sensitivity of CMOS-based imagers and scaling perspectives," *IEEE Trans. Electron Devices*, vol. 47, pp. 2110–2122, Nov. 2000.
[13] D. Knipp, H. Stiebig, J. Fölsch, F. Finger, and H. Wagner, "Amorphous silicon-based n-i-p-i-n structure for color detection," *J. Appl. Phys.*, vol. 83, no. 3, p. 1463, 1998.
[14] G. Wyszecki and W. S. Stiles, *Color Science*. New York: Wiley, 1982.
[15] O. Kluth, A. Löffl, S. Wieder, C. Beneking, L. Houben, B. Rech, H. Wagner, S. Hoffmann, R. Waser, J. A. Selvan, and H. Keppner, "Texture etched Al-doped ZnO: A new material for enhanced light trapping in thin-film solar cells," in *Proc. 26th IEEE PVSEC*, Oct. 1997, pp. 715–718.
[16] W. Luft and Y. Tuso, *Hydrogenated Amorphous Silicon Alloy Deposition Processes*. New York: Marcel Dekker, 1993.
[17] M. Born and E. Wolf, *Principles of Optics*. New York: Pergamon, 1980.
[18] Z. Knittl, *Optics of Thin Films*. New York: Wiley, 1976.
[19] D. Knipp, H. Stiebig, H. Fölsch, and H. Wagner, "Four-terminal color detector for digital signal processing," *J. Non-Cryst. Solids*, vol. 227–230, p. 1321, 1998.
[20] S. Mohajerzadeh, A. Nathan, and C. R. Selvakumar, "Numerical simulation of p-n-p-n color sensor for simultaneous color detection," *Sens. Actuators A*, vol. 44, p. 119, 1994.
[21] M. Ben Chouikha, F. Viénot, and G. N. Lu, "Characterization of a color sensitive photodetector implemented in BiCMOS technology," *Proc. SPIE*, vol. 3300, p. 198, 1998.

[22] P. G. Herzog, D. Knipp, H. Stiebig, and F. König, "Colorimetric characterization of novel multiple-channel sensors for imaging and metrology," *Proc. SPIE*, vol. 3648, p. 48, 1999.
[23] P. G. Herzog, D. Knipp, F. König, and H. Stiebig, "Performance of amorphous-silicon-based multiple-channel color sensors," *Proc. SPIE*, vol. 3963, p. 60, 2000.
[24] J. P. S. Parkkinnen, J. Hallikanainen, and T. Jaaskelainen, "Characteristic spectra of Munsell colors," *J. Opt. Soc Amer. A, Opt. Image Sci.*, vol. A 6, pp. 318–322, 1989.

Dietmar Knipp received the M.S. degree in electrical engineering from the University of Siegen, Siegen, Germany, in 1995 and the Ph.D. degree in electrical engineering from the Aachen University of Technology, Aachen, Germany, in 1999. While pursuing the Ph.D. degree, he worked on a-Si : H and its application for color sensors.

From 1999 to 2000, he was a Postdoctoral Fellow at the Research Center Jülich, Institute of Photovoltaics, Jülich, Germany, where he was engaged in work on optical sensors for metrology applications. Since 2000, he has been with Xerox Corporation, Palo Alto Research Center, Palo Alto, CA, where he is engaged in the development of organic electronics.

Patrick G. Herzog received the diploma degree in electrical engineering and the Ph.D. degree, both from the Aachen University of Technology, Aachen, Germany, in 1992 and 1997, respectively.

He is currently the Chief-Engineer of the Technical Electronics Institute at the Aachen University of Technology (RWTH), where he is responsible for research and industry projects in multispectral imaging, new sensor technologies, color management, and faithful color displays. Since the spring of 2000, he serves as CEO of the newly founded Color AIXperts GmbH. He is also a Lecturer in pulse electronics and a Member of CIE TC 8-03 "Gamut Mapping."

Helmut Stiebig received the Ph.D. degree in electrical engineering from the Aachen University of Technology, Aachen, Germany, in 1997.

Since 1992, he has been with the Research Center Jülich, Institute of Photovoltaics, Jülich, Germany. His research interests include the investigation of the optoelectronic properties of amorphous and microcrystalline silicon and related materials, numerical modeling, and the development of optical sensors.